Free Radical Conformations and Conversions in X-Irradiated Single Crystals of L-Cysteic Acid by Electron Magnetic Resonance and Density Functional Theory Studies

Kjell Tage Øhman* and Einar Sagstuen

Department of Physics, University of Oslo, P.O. Box 1048 Blindern, NO-0316 Oslo, Norway

Received: December 17, 2007; In Final Form: February 7, 2008

Single crystals of L-cysteic acid monohydrate were X-irradiated and studied at 295 K using EPR, ENDOR, and EIE techniques. Three spectroscopically different radicals were observed. These were a deamination radical reduction product (R1), and two oxidation products formed by hydrogen abstraction (radicals R2, R3). R2 and R3 were shown to exhibit the same chemical structure while exhibiting very different geometrical conformations. Cluster DFT calculations at the 6-31G(d,p) level of theory supported the experimental observations for radicals R1 and R2. It was not possible to simulate the R3 radical in any attempted cluster; hence, for this purpose a single molecule approach was used. The precursor radicals for R1, R2, and R3, identified in the low-temperature work on L-cysteic acid monohydrate by Box and Budzinski, were also investigated using DFT calculations. The experimentally determined EPR parameters for the low-temperature decarboxylated cation could only be reproduced correctly within the cluster when the carboxyl group remained in the proximity of the radical. Only one of the two observed low-temperature carboxyl anions (stable at 4 and 48 K) could be successfully simulated by the DFT calculations. Evidence is presented in support of the conclusions that the carboxyl reduction product already is protonated at 4 K and that the irreversible conversion between the two reduction products is brought forward by an umbrella-type inversion of the carboxyl group.

1. Introduction

The free radicals created in crystalline amino acids by ionizing radiation have been extensively studied during the last decades. This interest is partly due to the central role of amino acids in a large variety of biochemical systems and processes, and partly due to the widespread use of some amino acids as monitoring materials in Electron Paramagnetic Resonance (EPR) dosimetry. There exists a rich literature on the radiation chemistry of amino acids describing the formation of the pristine radicals at low temperatures and the pathway of these radicals to the stable room-temperature radicals.[1] Nevertheless, new radicals, formation pathways, and details of radical conformations are continuously being unraveled by new experiments using more advanced techniques and methods of analysis.[2] Even though most amino acids are fairly simple in composition, the small variations in molecular structures create subtle differences in radical formation processes that are not yet fully understood. It is important for the radiation chemistry of amino acids to understand the system-specific conditions for the different routes of radical formation; that is, why specific amino acid systems give rise to specific radicals. Acquiring such knowledge requires, however, that reliable and complete data from these systems exist. Unfortunately, a large part of the early radiation studies done on various solid state amino acid systems used only EPR spectroscopy, and not the adjunct Electron Nuclear DOuble Resonance (ENDOR) technique, which inherently has an enhanced signal resolution. Radical formation processes suggested on basis of investigations using EPR techniques alone may be uncertain. Furthermore, the interpretation of experimental data can now often be further supported by modern computational methods.[3]

The amino acid being the subject of the present work, L-cysteic acid, is an intermediate in the metabolic degradation of L-cysteine, which plays an important role in the structure of proteins. Furthermore, L-cysteic acid is also closely related to L-alanine, which is extensively used in radiation dosimetry. These two amino acids differ only by a sulfite group. In previous studies, irradiated single crystals of L-cysteic acid monohydrate were studied at low temperatures using ENDOR spectroscopy by Box and Budzinski,[4] and at room temperature using EPR spectroscopy by Ayscough and Roy.[5] In the low-temperature (4 K) ENDOR study, a decarboxylated radical (oxidation product) and a carboxyl anion radical (reduction product) were identified, both being well-known pristine radicals in the general solid state amino acid radiochemistry. The reduced carboxyl radical, however, exhibited two different EPR/ENDOR spectra, irreversibly interconnected upon thermal annealing from 4 to 48 K. A similar phenomena has to our knowledge previously been observed only in L-*o*-serine phosphate, where two geometrical conformations are connected through an irreversible umbrella-like inversion about the carboxyl carbon atom.[3] In the case of L-cysteic acid monohydrate, Box and Budzinski suggested that a proton transfer was responsible for the differences observed without considering the possibility for conformational changes. In the EPR room temperature study by Ayscough and Roy[5] only the deaminated reduction radical could be identified. The oxidative counterpart and other possible radicals were not detected due to the low resolution of the EPR spectra. No comparisons between the hyperfine coupling tensors and crystallographic data were made in either of these two previous studies, thus leaving some uncertainty with respect to their conclusions.

The objective of the present study was to acquire more complete experimental information on the room-temperature radicals of L-cysteic acid monohydrate, and to examine the

* Corresponding author. E-mail: k.t.ohman@fys.uio.no.

10.1021/jp711821c CCC: $40.75
Published on Web 04/16/2008

SCHEME 1: Molecular Structure of L-Cysteic Acid Monohydrate

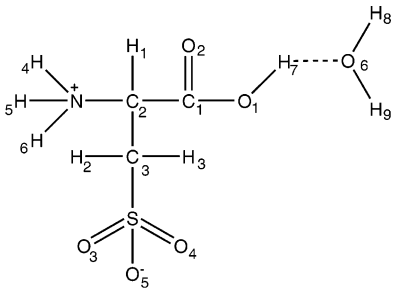

chemical and geometrical structures and hyperfine coupling properties of all proposed low- and room-temperature radicals using quantum computation simulations.

2. Experimental and Computational Methods

Single crystals of L-cysteic acid monohydrate (Sigma-Aldrich) were obtained from saturated aqueous solutions by slow evaporation at 45 °C ("normal" crystals). Partially deuterated crystals with the polar protons exchanged with deuterons were similarly prepared by repeated recrystallization from deuterium oxide (99%, Cambridge Isotope Laboratories). The unit cell of L-cysteic acid monohydrate is orthorhombic with space group symmetry $P2_12_12_1$ and $Z = 4$.[6] All the oxygen atoms and polar protons in the L-cysteic acid molecule are participating in intermolecular hydrogen-bonding interactions. The L-cysteic acid molecule is, as most solid state amino acids, in a zwitterionic form, where the amino group and the acidic sulfite group have one positive and one negative formal charge, respectively, whereas the carboxyl group carries no formal charge. The molecular structure of L-cysteic acid together with the water molecule and numbering system used in this study is shown in Scheme 1.

Identification of the crystal axes was made using a Weissenberg X-ray diffraction camera, and aided by the diffraction pictures the oscillation axis was aligned within 1° to one of the crystal axes. The crystals were subsequently transferred to coaxial quartz rods without loss of alignment, which could be confirmed from behavior of the site splitting resonances in the ENDOR spectra. The orthogonal Cartesian reference system in this work corresponds to the crystal axis system $\langle a, b, c \rangle$.

The crystals were irradiated at 295 K using 60 kV X-rays from a Philips PW 2188-tube with a Cr-anode operated at 40 mA. The total dose supplied was about 40 kGy. X-band EPR, ENDOR and EIE spectra were obtained using a BRUKER *Elexsys* 560 *SuperX* X-band EPR spectrometer connected to a Linux workstation running BRUKER *Xepr* software. For EPR spectroscopy, a 100 kHz modulation frequency was used together with a modulation amplitude of 0.1 mT and a microwave power of 1 mW (22 dB). For ENDOR/EIE spectroscopy, the BRUKER *DICE* system was set to generate a square-wave like frequency modulation of the rf-field at 10 kHz with a modulation depth of 150 kHz. A 150 W rf-amplifier from Amplifier Research was employed. The microwave power was set to about 12 mW (12 dB) for the ENDOR measurement. The cavity used for the EPR/ENDOR/EIE measurements was a standard BRUKER *EN801* cavity.

The proton hyperfine coupling (hfc) tensors were obtained from the experimental data using the *MAGRES* program.[7] This program assumes an isotropic *g*-tensor, which proved to be a good approximation for this study of L-cysteic acid monohydrate. EPR second-order perturbation spectrum-simulations were made using the program *KVASAT*.[8,9]

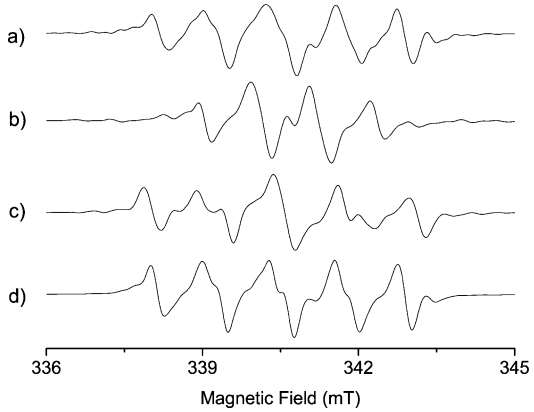

Figure 1. First-derivative EPR spectra of L-cysteic acid monohydrate single crystals X-irradiated and measured at 295 K: (a) nondeuterated ("normal") crystals with the external magnetic field along the $\langle a \rangle$ axis; (b) "normal" crystals with the external magnetic field along the $\langle b \rangle$ axis; (c) "normal" crystals with the external magnetic field along the $\langle c \rangle$ axis; (d) partially deuterated crystals with the external magnetic field along the $\langle a \rangle$ axis.

The EPR and ENDOR data were recorded through three orthogonal planes at 5° intervals of a total of 90° rotation. The Schonland ambiguity[10] was not solved experimentally; rather it was solved by the physical interpretation of the data, which was also the case with the inherit sign ambiguity due to the space group.

The Density Functional Theory (DFT) computations were performed on a 64- processor HP *Superdome* (Magnum) at the University of Oslo using the Symmetric Multi Processor (SMP) version of the quantum chemistry package *Gaussian 03* (G03), revision B.04.[11] Radicals of zwitterionic amino acids are difficult to simulate in unconstrained optimizations because the optimized molecules tend to bend excessively so as to create internal hydrogen bonds and internal proton transfers that are very unlikely to be real in a crystalline structure. These problems can be solved with the use of partially constrained cluster optimizations. Most of the radicals studied were optimized in cluster systems, in which the central radical molecule was surrounded by several other molecules at positions provided by crystallographic data.[12] Because the original crystallographic data[6] were obtained using X-ray diffraction, the C−H and O−H bonds generally tended to be too short. Small adjustments of all these bond lengths were made prior to any optimization of the cluster. These adjustments were based on a semiempirical (PM3) optimization of a very large L-cysteic monohydrate crystal system (24 molecules), where only the C−H and O−H bonds are optimized.

The size of the cluster was determined from the hydrogen-bonding scheme in the crystal structure, and the minimum requirement imposed was that all molecules participating in hydrogen bonding with the central radical molecule should be included in the cluster. Thus, the total size of this cluster consisted of five L-cysteic molecules and three water molecules surrounding the central radical molecule. This cluster was chosen as the template cluster in this study. Only the central radical molecule was optimized, whereas the other atomic coordinates in the system were frozen.

The method used for all computations was the hybrid functional B3LYP,[13−15] which is known to be reliable for organic radical systems. In this study the basis set 6-31G(d,p) was adopted for both the geometry optimization and the hyperfine coupling (hfc) tensor calculations. Hermosilla et al. found that even a small basis such as the 6-31G* gave

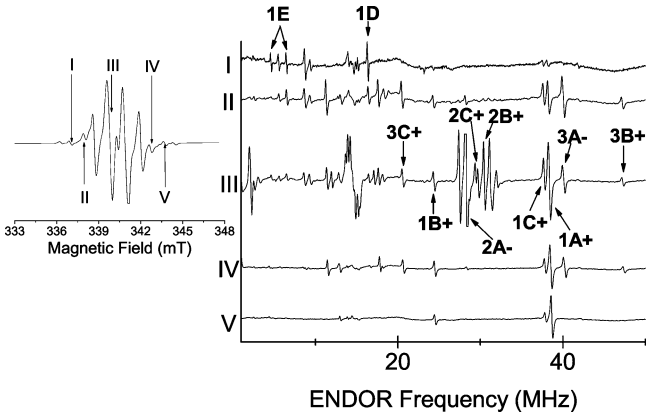

Figure 2. First derivative ENDOR spectra of X-irradiated L-cysteic acid monohydrate single crystals with the external magnetic field along the ⟨*b*⟩ axis (right panel), and the corresponding EPR spectrum (to the left). The various ENDOR spectra have been enumerated according to the position in the EPR spectrum to which the magnetic field was locked while recording the ENDOR. The assignment of + or − to each ENDOR line indicates whether the corresponding nuclear transition belongs to the $m_s = +1/2$ or the $m_s = -1/2$ energy level manifold.

satisfactory hyperfine tensors for several different molecules.[28,29] By using the 6-31G(d,p) basis instead of the 6-31G* basis, an additional set of polarization functions was added to the hydrogens. The inclusion of diffuse functions proved to be exceedingly problematic in these cluster calculations due to very slow scf convergence. Furthermore, adding diffuse functions to the optimization of the low-temperature carboxyl anion clusters discussed later did not seem to make any difference with respect to the results obtained.

The default *Gaussian 03* optimization routine and convergence criteria were used for the optimization, whereas the scf convergence criteria *scf = tight* was used for all single point and hfc tensor calculations. The atomic coordinates that were not to be optimized were frozen by the modRedundant option. In combination with the *noSymm* option of G03, the eigenvectors of the calculated dipolar coupling principal values and eigenvectors are directly comparable with the experimental results. The atomic spin densities were calculated using the *pop = npa* option, using natural population analysis.[16]

When eigenvectors of nearly axial dipolar coupling tensors, as commonly observed for some β-couplings, are compared, only the axial eigenvectors should be used because large uncertainties are connected to the directions associated with the pair of nearly degenerated eigenvalues. Also, comparing measurements made at room temperature with the static DFT simulations is less reliable than similar comparisons made with measurements made at low temperatures due to thermal effects that are not taken into account in the simulations.

3. Experimental Results and Analysis

EPR spectra recorded from normal and partially deuterated crystals irradiated at 295 K are shown in Figure 1. The only observable difference between the two types of crystals (Figure 1a,d) is the apparent absence of some very weak flanking resonance lines in the spectra from normal crystals together with minor changes in the central resonance ($g \approx 2$ region). As compared to Figure 1a,c, Figure 1b shows a smaller number of resonance lines and a significantly smaller spectrum width; both indicate the existence of at least one major anisotropic coupling. From the spectra in Figure 1, the assumption of isotropic *g*-factors for the tensor analysis appears to be justified.

Most ENDOR lines could be detected at all orientations when the magnetic field was locked onto the central resonance lines in the EPR spectra as shown in Figure 2 III. The intensity ratio between the low-frequency and the high-frequency branches of some ENDOR lines was, however, strongly dependent on the actual magnetic field position used to detect the ENDOR. This phenomenon can to some extent be used to determine the relative signs of the couplings (see below).[2,17] All detected ENDOR lines were due to interactions with protons, except for one resonance being due to a nitrogen interaction. Hyperfine coupling tensors could not be established from all the observed ENDOR lines because it was not possible to follow some of the lines through all three orthogonal planes of rotation.

As shown in Figure 3, three distinct sets of ENDOR Induced EPR (EIE) spectra, R1, R2, and R3, were obtained whenever the magnetic field was aligned with either of the crystallographic axes. Also comparing Figures 1 and 3 shows that the quintet/quartet resonance due to radical R2 is the dominant feature of the EPR spectra.

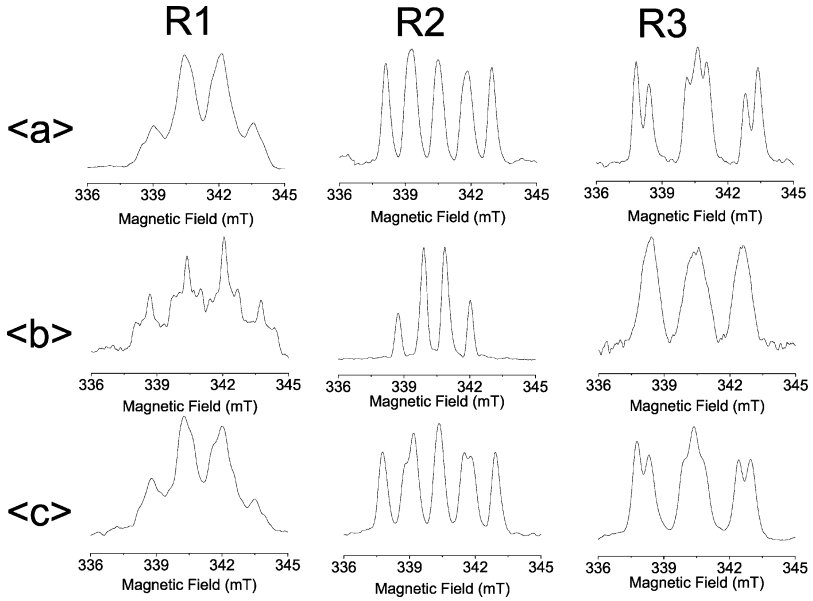

Figure 3. Distinct EIE spectra observed with the magnetic field aligned along each of the different crystallographic axes. The different sets of EIE spectra were assigned to the three radical species R1, R2, and R3. The EIE spectra are recorded from 333 to 347 mT.

TABLE 1: Experimental Hyperfine Coupling Tensors for Radical R1 in Single Crystals of L-Cysteic Acid Monohydrate X-Irradiated and Measured at 295 K Together with the DFT Computed Hyperfine Coupling Tensors[a]

tensor	principal values (MHz)	isotropic value (MHz)	anisotropic values (MHz)	eigenvectors ⟨a⟩	eigenvectors ⟨b⟩	eigenvectors ⟨c⟩
βH (1A) exp	46.81(3)		5.53(4)	−0.053(1)	−0.996(20)	0.065(1)
	38.78(3)	41.28(2)	−2.50(4)	−0.060(0)	−0.061(2)	−0.996(2)
	38.26(2)		−3.02(3)	−0.996(1)	0.057(1)	0.057(20)
H (NH3) calc		39.7[b]				
βH (1B) exp	22.73(2)		7.84(3)	−0.462(1)	0.804(25)	−0.372(11)
	11.31(3)	14.89(2)	−3.58(4)	−0.386(1)	0.195(16)	0.901(5)
	10.63(3)		−4.26(4)	0.798(2)	0.560(7)	0.220(30)
H2 calc	20.37		7.89	−0.435	0.750	−0.498
	8.83	12.49	−3.65	−0.650	0.120	0.750
	8.23		−4.25	0.623	0.650	0.435
βH (1C) exp	56.43(2)		7.59(2)	0.581(1)	−0.125(19)	0.803(2)
	45.30(3)	48.84(1)	−3.54(3)	0.094(1)	−0.970(4)	−0.220(23)
	44.79(2)		−4.05(2)	0.808(1)	0.204(13)	−0.552(5)
H3 calc	58.78		7.73	0.504	−0.083	0.860
	47.33	51.05	−3.72	0.701	−0.542	−0.463
	47.05		−4.00	0.505	0.836	−0.215
αN (1E) exp	*c*	∼(−)9[d]	*c*			
N calc		−5.11				

[a] Uncertainties are given at the 95% confidence level in the last digit(s) of the quoted values. [b] Estimate of the isotropic value obtained by using the mean value of the isotropic values of each of the three amino protons. [c] Anisotropy could not be properly resolved. [d] Isotropic eigenvalue estimated from ENDOR spectra with the external magnetic field aligned along the crystal axes.

TABLE 2: C2−N, C2−H2, and C2−H3 Crystallographic Directions of L-Cysteic Acid Monohydrate Compared with the Experimental Eigenvectors from the R1, R2, and R3 Radicals Corresponding to the Maximum Anisotropic Coupling

crystallographic directions		experimental eigenvector			angular deviations (deg)		
C2-N		1A	2A	3A	1A	2A	3A
⟨a⟩	−0.116	−0.053	0.063	0.469			
⟨b⟩	−0.989	−0.996	−0.998	−0.634	3.8	10.8	58.5
⟨c⟩	0.083	0.065	0.025	−0.615			
crystallographic directions		experimental eigenvector			angular deviations (deg)		
C2-H2		1B	2B	3B	1B	2B	3B
⟨a⟩	−0.537	−0.462	−0.430	−0.679			
⟨b⟩	0.774	0.804	0.752	0.727	5.1	11.4	15.8
⟨c⟩	−0.334	−0.372	−0.500	−0.103			
crystallographic directions		experimental eigenvector			angular deviations (deg)		
C2-H3		1C	2C	3C	1C	2C	3C
⟨a⟩	0.616	0.581	0.587	0.699			
⟨b⟩	−0.210	−0.125	−0.021	−0.235	5.9	11.4	6.9
⟨c⟩	0.758	0.803	0.809	0.675			

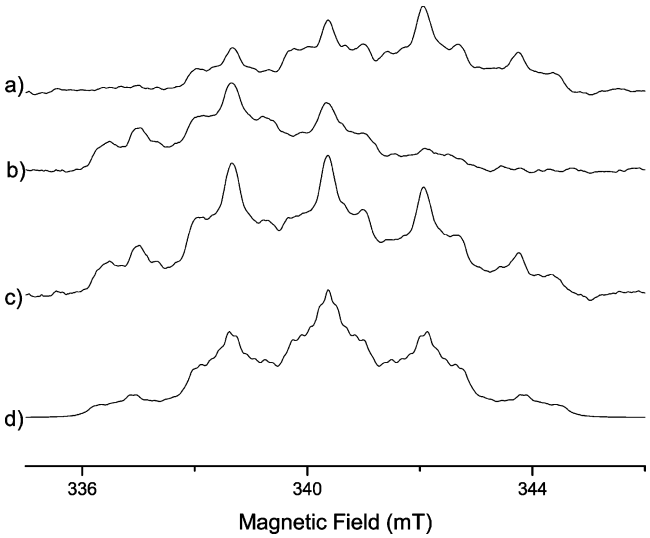

Figure 4. (a, b) EIE spectra obtained by monitoring a high-frequency and a low-frequency ENDOR line from radical R1 with the magnetic field aligned along the ⟨*b*⟩ axis. (c) EIE spectrum obtained by adding the two spectra in (a) and (b). (d) Simulated EPR absorption spectrum used the experimental hfc tensors and observed resonance line positions (couplings 1D and 1E) at the ⟨*b*⟩ axis for radical R1.

To verify that the radicals R1, R2, and R3 indeed are the successors of the low-temperature radicals observed by Box and Budzinski,[4] one experiment was performed in which an L-cysteic acid monohydrate single crystal was X-irradiated at 77 K followed by slow warming to room temperature. This resulted in the same EPR/ENDOR spectra at room temperature as those observed immediately after X-irradiation at 295 K.

3.1. Radical R1 Characterization. Locking the magnetic field to different positions in the EPR spectrum (Figures 2I−V) indicates that ENDOR lines 1A−1E all should be assigned to one radical: R1. These ENDOR lines also give rise to similar EIE spectra, as shown in Figure 3. The weak proton and nitrogen resonance lines 1D and 1E, respectively, could only be observed at a few orientations of the magnetic field; thus the corresponding hfc tensors could not be established. Couplings 1A, 1B, and 1C (Table 1) are all due to proton interactions and can be characterized as *β*-proton interactions due to the near axial symmetry of their eigenvalues and the small anisotropy. Only the interaction yielding coupling 1A is easily exchangeable with deuterons. As shown in Table 2, there is good agreement between the crystallographic directions C2−N, C2−H2, and C2−H3 and the experimental eigenvectors corresponding to the maximum anisotropic principal values of couplings 1A, 1B, and 1C, respectively.

The complete EIE spectrum due to R1 (obtained by adding EIE spectra from monitored high-frequency and low-frequency

SCHEME 2: Chemical Structure of Radical R1

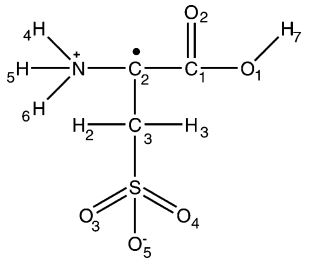

SCHEME 3: Chemical Structure of Radical R2, R3

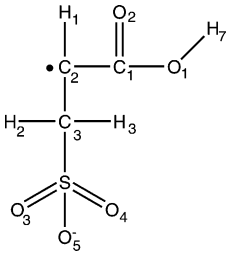

ENDOR lines as shown in Figure 4a−c) can only be simulated satisfactorily (Figure 4d) if the exchangeable coupling 1A is assumed to be due to three equivalently coupled β-protons of a rotating amino group. The observed eigenvalues for 1A are also similar to those observed at 295 K for the freely and fast rotating amino group of the R1 radical in α-glycine.[18]

Similar to α-glycine[18] the rapid rotor in L-cysteic acid induces efficient electron−nuclear flip-flop W_{1x} cross relaxations in such a way that it is possible to determine the relative signs of the eigenvalues from the relative intensities of the resonance lines in Figure 2I,V. The intensity behavior from these figures suggests that the eigenvalues of the proton couplings 1A, 1B, and 1C all have the same signs.

It is concluded from the analysis above that the majority of the unpaired electron in radical R1 must be located at C2 and the radical structure must exhibit the structure shown in Scheme 2, formed by the net abstraction of H1 from the L-cysteic acid molecule.

The isotropic values for 1B and 1C, 15 and 49 MHz, respectively, may be compared to those calculated using the Heller−McConnell relation[19]

$$a_{\mathrm{iso}}^{\beta} = (B_0 + B_2 \cos^2 \theta)\rho^{\pi}$$

where B_0 and B_2 are constants assumed to be 0 and 126 MHz, respectively.[20] θ is the dihedral angle between the C−H_β bond and the axis of the lone electron orbital (LEO), and ρ^{π} is the unpaired spin density of the LEO. If the (broken) C2−H1 bond is chosen as an approximation for the axis of LEO, then according to the Heller−McConnell relation the 1B and 1C isotropic eigenvalues are calculated to exhibit similar values (46−44 MHz for $\rho^{\pi} = 1$), because the dihedral angles H1−C2−C3−H2 and H1−C2−C3−H3 are nearly equal (54°/53°). This result disagrees with the experimental data for 1B and 1C. On the other hand, the cluster DFT calculations for the R1 radical, discussed later, do indeed give hyperfine coupling tensors for H2 and H3 in good agreement with experimental data for 1B and 1C.

3.2. Radical R2 Characterization. Similar to the radical R1 ENDOR lines, the resonance lines 2A, 2B, and 2C were assigned to radical R2 by locking the magnetic field to different positions in the EPR spectrum (Figure 2) and also by EIE techniques. Other ENDOR lines with EIE spectra almost identical to those of radical R2 could also be observed; they shadowed the R2 ENDOR lines through the three planes of rotation with only minor shifts in resonance frequency. These resonance lines are therefore assumed to represent minor conformation variations of the R2 radical. At least two such conformations (R2*, R2**) of R2 were observed. The couplings 2A, 2B, and 2C are all due to protons interactions, and from their anisotropic behavior, it appears that coupling 2A exhibits α-character and couplings 2B and 2C are typical of β-type interactions. None of the observed couplings seems to be easily exchangeable with deuterons.

When the eigenvectors corresponding to the maximum anisotropic principal value of couplings 2A, 2B, and 2C (Table 3) are compared with those of couplings 1A, 1B, and 1C,

TABLE 3: Experimental Hyperfine Coupling Tensors for Radical R2 in Single Crystals of L-Cysteic Acid Monohydrate X-Irradiated and Measured at 295 K Together with the DFT Computed Hyperfine Coupling Tensors[a]

tensor	principal values (MHz)	isotropic value (MHz)	anisotropic values (MHz)	eigenvectors ⟨a⟩	⟨b⟩	⟨c⟩
αH (2A) exp.	−26.10 (4)		29.38(5)	0.063(0)	−0.998(0)	0.025(1)
	−54.34 (5)	−55.48 (3)	1.14(6)	0.750(1)	0.031(1)	−0.661(0)
	−86.00 (5)		−30.52(6)	0.658(0)	0.061(0)	0.750(1)
H1 calc	−24.95		33.24	0.107	−0.994	0.013
	−60.80	−58.19	−2.61	0.811	0.079	−0.580
	−88.82		−30.63	0.575	0.072	0.815
βH (2B) exp	35.43(4)		7.11(4)	−0.430(2)	0.752(67)	−0.500(3)
	25.01(4)	28.32(2)	−3.31(4)	−0.043(1)	0.536(29)	0.843(40)
	24.52(4)		−3.80(4)	0.902(2)	0.384(15)	−0.198(63)
H2 calc	30.32		7.75	−0.380	0.724	−0.576
	18.75	22.57	−3.82	0.761	−0.109	−0.640
	18.64		−3.93	0.526	0.682	0.509
βH (2C) exp	39.67(3)		7.37(4)	0.587(2)	−0.021(71)	0.809(2)
	28.76(6)	32.30(2)	−3.54(6)	0.013(2)	−0.999(2)	−0.035(87)
	28.48(3)		−3.82(4)	0.809(1)	0.031(50)	−0.587(34)
H3 calc	43.96		7.87	0.462	−0.053	0.885
	32.42	36.09	−3.67	0.834	−0.313	−0.454
	31.89		−4.20	0.302	0.948	−0.100

[a] Uncertainties are given at the 95% confidence level in the last digit(s) of the quoted values.

TABLE 4: Experimental Hyperfine Coupling Tensors for Radical R3 in Single Crystals of L-Cysteic Acid Monohydrate X-Irradiated and Measured at 295 K Together with the DFT Computed Hyperfine Coupling Tensors[a]

tensor	principal values (MHz)	isotropic value (MHz)	anisotropic values (MHz)	eigenvectors ⟨*a*⟩	eigenvectors ⟨*b*⟩	eigenvectors ⟨*c*⟩
αH (3A) exp	−29.97 (7)		30.62(8)	0.469(1)	−0.634(2)	−0.615(1)
	−62.17 (5)	−60.59(4)	−1.58(6)	0.562(1)	0.751(1)	−0.346(2)
	−92.79 (8)		−32.20(9)	0.681(1)	−0.184(1)	0.708(1)
H1 calc	−23.27		30.54	−0.454	0.666	0.593
	−55.36	−53.81	−1.55	0.670	0.693	−0.265
	−82.81		−29.00	0.588	−0.277	0.760
*β*H (3B) exp	69.62 (2)		7.46(2)	−0.679(1)	0.727(7)	−0.103(5)
	58.97 (2)	62.16(1)	−3.19(2)	0.463(1)	0.533(5)	0.708(7)
	57.90 (2)		−4.26(2)	0.570(2)	0.433(8)	−0.699(8)
H2 calc	69.82		7.23	−0.576	0.814	−0.074
	59.38	62.59	−3.21	0.370	0.340	0.865
	58.57		−4.02	0.730	0.471	−0.496
*β*H (3C) exp	21.70 (3)		7.81(4)	0.699(1)	−0.235(20)	0.675(8)
	10.44 (3)	13.89(2)	−3.45(4)	0.260(2)	0.963(4)	0.066(27)
	9.54 (3)		−4.35(4)	0.666(2)	−0.130(20)	−0.735(2)
H3 calc	13.64		6.62	0.567	−0.293	0.770
	4.23	7.09	−2.79	0.796	0.437	−0.420
	3.19		−3.83	−0.214	0.850	0.481

[a] Uncertainties are given at the 95% confidence level in the last digit(s) of the quoted values.

respectively, it appears that radical R2 must have the same radical center as radical R1 (i.e., C2). For this to be possible, a deamination process must have occurred, as shown in Scheme 3, and subsequently the H1−C2 bond must have realigned to become nearly parallel to the old N−C2 bond. A spin population of 0.76 on C2 is found using both the McConnell relation[21]

$$a_{iso} = Q_{iso}\rho^{\pi}$$

with $Q_{iso} = -73.4$ MHz and the Gordy−Bernhard relation[22,23]

$$a^{x}_{dip} = Q_{dip}\rho^{\pi}$$

with $Q_{dip} = 38.7$ MHz (x is along the >C−H bond direction) together with the eigenvalues from the α-coupling 2A. Similar values of the spin populations from these to relations indicates a planar radical center.[24] Most likely there is some spin delocalization in the π-conjugated system between the $2p_\pi$ orbitals of C2 and the carboxyl oxygens. The isotropic eigenvalues for 2B and 2C are 28 and 32 MHz. Using the Heller−McConnell relation with B_0 and B_2 constants of 0 and 126 MHz together with a spin density of $\rho^{\pi} = 0.76$ and dihedral angles −38° and +69° obtained by using the 1A eigenvector of the intermediate eigenvalue and the crystallographic C3−H3 and C3−H2 interspin vectors, the isotropic values can be calculated to 58 and 12 MHz. Thus, similar to the R1 radical, the crystallographic data do not represent the molecular structure after radical formation sufficiently well to properly describe the observed experimental values. On the other hand, the cluster DFT calculation for R2, discussed later, gives hyperfine coupling tensors in far better agreement.

3.3. Radical R3 Characterization. Three ENDOR lines associated with the triplet/quintet EIE spectra of radical R3 could be detected, and subsequently three hfc tensors 3A, 3B, and 3C were established. All interactions are due to proton couplings. From their anisotropic behavior it can readily be seen that coupling 3A exhibits α-character and couplings 3B and 3C both exhibit *β*-character (Table 4). None of these couplings are easily exchanged with deuterium. With two nonexchangeable *β*-protons in addition to a large α-proton, only a radical centered at C2 is possible. Furthermore, the absence of any observable interaction to the amino group suggests that radical R3 must be chemically similar to radical R2 (Scheme 3), also formed by a net deamination process. In Table 2, the eigenvectors corresponding to the maximum anisotropic eigenvalues of couplings 3A, 3B, and 3C are compared with the C2−N, C2−H2, and C2−H3 crystallographic directions of L-cysteic acid monohydrate. This comparison reveals that the couplings 2A and 3A, and thus the position of H1, constitute the major difference between the R2 and R3 radicals. Furthermore, an angular difference of 48° is found by comparing the eigenvectors of the corresponding intermediate anisotropic principal values of tensors 3A and 2A. These eigenvectors represent the axis of the LEO of R3 and R2.[24] A spin population of 0.83 on C2 is obtained when using the McConnell[21] relation and a spin population of 0.79 when using the Gordy−Bernhard relation.[22,23]

4. Density Functional Theory (DFT) Calculations

4.1. Computational and Mechanistic Results for Radical R1 and Its Precursor. A decarboxylation radical product was observed in the low-temperature study by Box and Budzinski.[4] This is a well-known low-temperature product in irradiated amino acids, commonly believed to follow from a pristine oxidation event by elimination of CO_2.[1] This decarboxylation product is in turn assumed to be the precursor for hydrogen abstraction radicals often observed in room-temperature studies, as, e.g., radical R1 in the present study.

The decarboxylation radical cluster was prepared into two different systems from the template cluster described above. System A was prepared by eliminating the hydroxyl proton from the central molecule and elongating the bond between the carboxyl group and the α-carbon by 1 Å. In addition, the carboxylic group was made linear to provide faster optimization convergence. System B was prepared by removing the entire protonated carboxyl group from the cluster. The total charge of both systems was set to zero. The optimized structures and the relevant hfc tensors of these cluster calculations are shown in Figure 5 and Table 5. The coupling tensors calculated for system A are in good agreement with the experimental data published by Box and Budzinski.[4] Furthermore, the spin

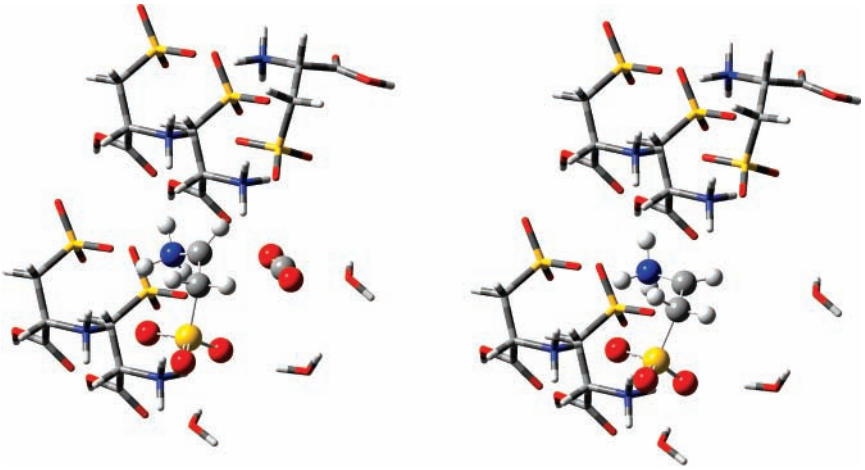

Figure 5. DFT optimized geometries of the L-cysteic acid decarboxylated cation observed after X-irradiation and EPR/ENDOR measurements of L-cysteic acid monohydrate crystals at 4 K. The ball-and-stick molecules are included in the optimization routine, the others are frozen. Left: optimized system A with the carboxylic group present. Right: optimized system B with the carboxylic group completely removed.

TABLE 5: Comparison between the Experimental and Calculated Eigenvalues Together with the Eigenvector Angular Deviation δ for the Low-Temperature (4 K) Decarboxylated Cation[4,a]

experimental			system A			system B	
iso (MHz)	aniso (MHz)	iso (MHz)	aniso (MHz)	δ (deg)	iso (MHz)	aniso (MHz)	δ (deg)
	36.6		40.0	6.4		39.1	58.4
−66.2	1.2	−72.3	−1.5	7.3	−66.6	−1.8	58.4
	−37.8		−39.0	6.1		−37.2	2.7
	7.8		9.0	3.9		9.1	11.3
132.4	−2.2	128.0	−3.0	3.2	79.3	−4.0	24.2
	−5.6		−5.9	6.3		−5.1	9.0
	11.9		12.8	12.7		11.2	6.0
86.5	−4.9	92.4	−4.8	15.8	69.2	−3.0	8.8
	−7.1		−8.1	9.4		−8.2	7.0

[a] System A is the geometry optimized structure including the CO_2 molecule, and system B is the geometry optimized structure without the CO_2 molecule, both shown in Figure 4. The level of theory used is B3LYP/6-31G(d,p) for A and B.

population on C2 was calculated to 0.94 in system A, similar to that was found for the low-temperature decarboxylated radical in L-*o*-serine phosphate (0.95).[3] It is interesting to observe that the calculation for system B with the CO_2 group completely eliminated from the cluster does not give the correct hfc tensors for R1. The repositioning of H1 is in this case not hindered by the CO_2 molecule as in system A, and the optimized position of H1 in system B is far from to the position deduced from the experimental data.

The room-temperature radical R1 observed in this study was prepared from the template cluster with the H1 atom eliminated from the central molecule. The total charge of the system was set to 0. The results are given in Table 1 and Figure 6. The hfc's are in excellent agreement with the experimental data. The tensor associated with the rotating amino group could not be simulated due to the nondynamical nature of the calculations. However, an estimate of the isotropic value was obtained by using the mean value of the calculated isotropic values of each of the three amino protons. This estimate gives an isotropic value of 39.7 MHz, which is close to the experimental average value of 41.3 MHz for 1A.

4.2. Computational and Mechanistic Results for Radicals R2, R3, and the Precursor Radicals. In the low-temperature study by Box and Budzinski,[4] two different carboxyl anion radicals were reported, irreversibly connected upon thermal annealing from 4 to 48 K. Box and Budzinski[4] tentatively suggested a proton transfer to the carboxylic group during the annealing from 4 to 48 K to account for the changes in the coupling tensor of the H1 interaction. However, the characteristics of these changes are peculiar. That is, the isotropic coupling value decreased and the anisotropic eigenvalues increased, while the eigenvectors remained almost unchanged.

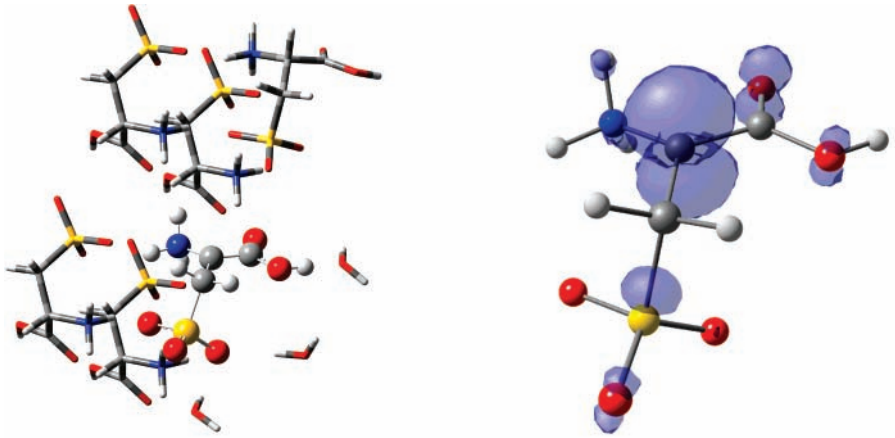

Figure 6. Left: optimized structure of the radical R1 simulation. The R1 radical is observed after X-irradiation and EPR/ENDOR measurements of L-cysteic monohydrate at 295 K. The ball-and-stick molecules are included in the optimization routine, the others are frozen. Right: isospin surfaces at 0.007 au of the optimized R1 radical.

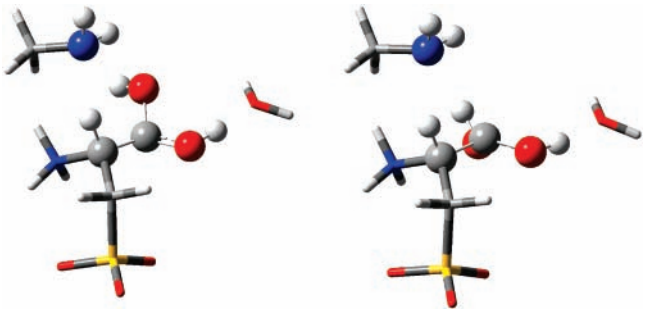

Figure 7. Two conformations found for the low-temperature protonated carboxylic anion of L-cysteic monohydrate, which are distinguished by inversed pyramidal geometries of the carboxyl groups. The atoms indicated by balls were included in the optimization routine, the others are frozen. The structure to the right gives hfc-tensors in good agreement with those previously published, which were recorded at 48 K.

This striking mode of variation was recently observed upon annealing a protonated carboxylic anion in L-*o*-serine phosphate from 10 to 77 K;[3] however, the experimental data and associated DFT calculations for this system suggested a geometry change by an inversion of the pyramidal carboxyl group and not a proton transfer because the proton already had been transferred at 10 K.

It turned out not to be possible to simulate either of the suggested structures[4] for the low-temperature one-electron reduced radicals using the template cluster system. For the 48 K protonated anion, the proton having been transferred to O2 always spontaneously transferred back to the donor amino group. By this, the model efficiently back-transformed into the proposed 4 K carboxyl anion radical of Box and Budzinski.[4] However, upon this back-transformation the unpaired spin became delocalized unevenly over several carboxyl groups in the cluster when the formal charge on the carboxyl oxygen was negative by one unit charge. This is in contradiction with the experimental data[4] and is probably due to some boundary effects associated with the cluster.

Therefore, to simulate these carboxyl one-electron reduced radicals, a different approach was used. A single L-cysteic acid molecule was used rather than the template cluster. The hydroxyl group O1−H and the carbonyl oxygen O2 of the single molecule were hydrogen bonded to a water molecule and an aminomethyl group, respectively, in an attempt to reproduce the hydrogen-bonding scheme of the L-cysteic acid carboxyl group as described by crystallographic data. Only the $C_\alpha H$ group, the carboxyl group and the neighboring amino group were free to relax upon geometry optimization. Two different molecular conformations were found after optimization with slightly different initial carboxyl pyramidal geometries and by protonation at O2 of the carboxyl anion from the neighboring amino group. As is evident from the visualization in Figure 7, these two conformations are connected by an inversion of the carboxylic group. It should be noted that with the starting structure as described above, it was not possible to determine an optimized structure before protonation, because protonation at O2 inevitably and spontaneously occurred during the optimization. Hence, the low-temperature 4 K nonprotonated carboxyl anion reportedly observed by Box and Budzinski[4] could not be simulated in this scheme. On the other hand, the simulation for the low-temperature 48 K protonated carboxyl anion now yielded calculated hfc tensors in very good agreement with the available data, as shown in Table 6.

TABLE 6: Comparison between the Experimental and Calculated Eigenvalues Together with the Eigenvector Angular Deviation δ for the Low-Temperature 48 K Protonated Carboxyl Anion[4,a]

	experimental		DFT		
tensor	isoo (MHz)	aniso (MHz)	iso (MHz)	aniso (MHz)	δ (deg)
H1		11.3		11.8	6.0
	48.7	−4.9	54.8	−5.3	7.3
		−6.5		−6.5	7.0
O2−H		20.3		22.2	4.3
	35.3	−7.3	36.5	−8.1	7.4
		−12.5		−14.1	8.5

[a] The level of theory used is B3LYP/6-31G(d,p).

These carboxyl anion radicals are known to be the precursors for the deaminated radicals observed at room temperature. Examples of such species are the R2 and R3 radicals in the present study. The room-temperature radical R2 found in this study was simulated in the template cluster, in which the amino group was eliminated from the cluster. The total charge of the system was set to one negative unit charge. After the optimization convergence, the H1−C2 bond was found along the old N−C2 bond, as shown in Figure 8. The spin density on C2 was calculated to 0.80, all in accordance with the experimental results discussed above (0.76). The hfc couplings are also in good agreement with those experimentally determined, as shown in Table 3.

The geometrical and magnetic properties of room-temperature radical R3, however, could not be reproduced in any attempted

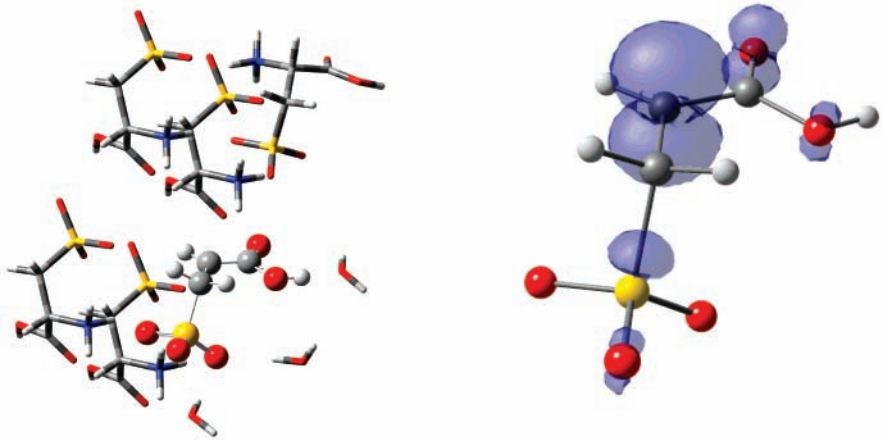

Figure 8. Left: optimized structure of the R2 radical simulation. The R2 radical is observed after X-irradiation and EPR/ENDOR measurements of L-cysteic acid monohydrate at 295 K. The ball-and-stick molecules are included in the optimization routine, the others are frozen Right: isospin surfaces at 0.007 au of the R2 radical.

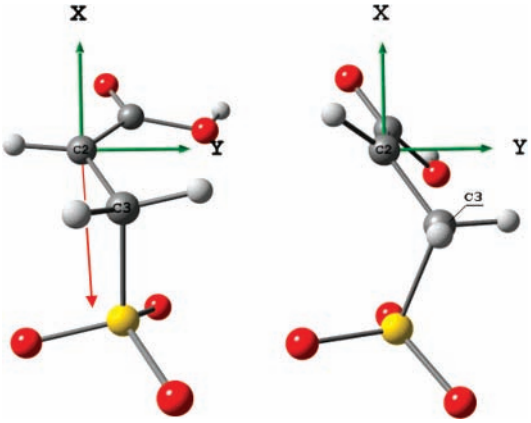

Figure 9. Left: optimized structure R2 structure taken from the R2 cluster simulation shown in Figure 8, left panel. The red arrow indicates the (−0.86, 0.03, −0.51) vector used to create the radical R3 structure. Right: model for radical R3, derived from the R2 structure as described in the text.

cluster calculation. To reproduce the R3 hfc tensors, it was commented above that the direction of the C2−H1 bond seems to constitute the major difference from the R2 structure (Table 2). Thus, a single molecule model can be constructed for R3 by rotating the entire R2 radical 47° clockwise around the vector (−0.86, +0.03, −0.51), where this angle and vector are found from a comparison of the α-tensors from R2 and R3. A subsequent 20° twist around the C2−C3 bond keeping the carboxyl group fixed yields the model shown in Figure 9, and the corresponding single-molecule DFT calculations produces the hfc tensors that are presented in Table 4.

5. Summary and Discussion

The room-temperature experiments and the DFT calculations presented in this study have shown that the radiation behavior of solid L-cysteine monohydrate follows the traditional reaction pathway from its pristine low-temperature radicals.[1] An unusually high number of conformations of the deamination radical, R2, R2*, R2**, and R3, was found at room temperature. R2 and R3 exhibited very different EIE spectra, and only a complete investigation with ENDOR and DFT simulations could establish that these two radicals only represent two geometrical conformations of the same chemical species. It does not seem that the room-temperature radical conformations R2 and R3 results from two different precursor radicals, something that might be speculated because Box and Budzinski described two one-electron reduced carboxyl radicals at 4 and 48 K.[4] To investigate this closer, L-cysteic acid monohydrate single crystals were X-irradiated at 77 K and then slowly warmed up to 295 K. The EPR/ENDOR spectra subsequently recorded from these crystals were similar to those obtained from L-cysteic acid monohydrate single crystals X-irradiated and measured at 295 K. X-irradiation at 77 K verified that only the 48 K protonated carboxyl anion radical conformation is present at 77 K and also was the only species that was transformed upon annealing (at about 160 K) into the R2, R2*, R2** and R3 deaminated radicals.

The DFT simulations for the low-temperature decarboxylated cation showed that the carboxyl group needs to be trapped in the proximity of the radical to reproduce the experimental data. This is different from the situation for the room-temperature deaminated radical R2 cluster, in which the detached amino group had to be completely eliminated.

The DFT simulations for the O2-protonated carboxyl anion at 48 K suggest that the radical conformation is close to that depicted in the right panel of Figure 7. No conclusive answer to the chemical and geometrical structure of the low-temperature carboxyl anion at 4 K can be offered, but it is possible and probable that the structure is somewhat similar to that depicted in the left panel of Figure 7, with O2 already protonated even at 4 K. The rationale for this conclusion is that the changes reported by Box and Budzinski[4] in anisotropic and isotropic values of the hyperfine coupling to H1 between 4 and 48 K for this radical are characteristic of those expected upon an inversion about the radical center. This inversion process is discussed in detail in the previous L-*o*-serine phosphate paper.[3] It is also notable that the DFT calculation predicts a spontaneous proton transfer from a neighboring amino group to O2 of the carboxyl anion radical; however, this proton transfer was not reported in the original low-temperature experiments.[4] The computed hyperfine coupling tensors for the 4 K carboxyl anion depicted in the left panel of Figure 7 are given in Table 7. It appears that the isotropic value for the H4 coupling is too small as compared to experimental data, but the computationally more reliable anisotropic eigenvalues are in better agreement. For the incoming proton, the DFT calculation indicates a small isotropic coupling; hence, it is possible that this coupling was not detected in the previous work.[4] Furthermore, the neighboring L-cysteine monohydrate amino protons are much closer to the carbonyl group (2.05 Å C−O···H−N) than in the case of L-*o*-serine phosphate (2.94 Å C−O···H−N). In L-*o*-serine phosphate the proton transfer had already occurred at 4 K, and it is possible that this have happened for the L-cysteine anion radical at 4 K as well.

TABLE 7: Comparison between the Experimental and Calculated Eigenvalues Together with the Eigenvector Angular Deviation δ for the Low-Temperature 4 K Protonated Carboxyl Anion[4,a]

	experimental		DFT		
tensor	iso (MHz)	aniso (MHz)	iso (MHz)	aniso (MHz)	δ (deg)
H1		7.4		9.0	10.4
	68.6	−1.6	46.7	−3.1	6.9
		−5.8		−5.9	6.4
O2−H				20.7	
			11.4	−8.5	
				−12.2	

[a] The level of theory used is B3LYP/6-31G(d,p).

The results presented in the current work warrant a comment to the general radical processes taking place in amino acids. In previous work, the compound 2-aminoethyl hydrogen sulfate (AES) was investigated.[25,26] In this compound, only a SO_3^{2-} and a carbon-centered radical localized on C3 (see Scheme 1) were detected at room temperature, no deamination product was detected. AES is the decarboxylated analogue of cysteic acid; that is, the carboxyl group of cysteic acid has been replaced with a hydrogen. In cysteic acid, no sulfur-centered radicals and no C3-centered radical have been observed, not at any temperature studied. The differences in radiation response between these two systems clearly illustrate the crucial importance of the carboxyl group both as the locus for electron capture and for electron loss in amino acids. A parallel observation is made by comparing the radical formations in L-*o*-serine phosphate[3] and phosphoryl ethanolamine (PEA),[27] the corresponding decarboxylated analogue of L-*o*-serine phosphate. In PEA, phosphate centered radicals assumedly formed by reductive dephorphorylation were detected, no similar processes have been observed in L-*o*-serine phosphate.

Acknowledgment. The Scientific Computer Group at University of Oslo and the Norwegian Metacenter for Computational Science (NOTUR) are gratefully acknowledged for grants of computer time.

References and Notes

(1) Sagstuen, E.; Sanderud, A.; Hole, E. O. *Rad. Res.* **2004**, *162*, 112.
(2) Sagstuen, E.; Hole, E. O.; Haugedal, S. R.; Nelson, W. H. *J. Phys. Chem. A* **1997**, *101*, 9763.
(3) Øhman, K. T.; Sagstuen, E.; Sanderud, A.; Hole, E. O. *J. Phys. Chem. A* **2006**, 9585.
(4) Box, H. C.; Budzinski, E. E. *J. Chem. Phys.* **1974**, *60*, 3337.
(5) Ayscough, P. B.; Roy, A. K. *Trans. Faraday Soc.* **1968**, *64*, 582.
(6) Hendrickson, W. A; Karle, J. *Acta Crystallogr. B* **1971**, 427.
(7) Nelson, W. H. *J. Magn. Reson.* **1980**, *38*, 71.
(8) Sagstuen, E.; Lund, A.; Itagaki, Y.; Maruani, J. *J. Phys. Chem. A* **2000**, *104*, 6362.
(9) Sagstuen, E.; Hole, E. O.; Haugedal, S. R.; Lund, A.; Eid, O. I.; Erickson, R. *Nukleonika* **1997**, *42*, 353.
(10) Schonland, D. S. *Proc. Phys. Soc. London A* **1959**, *73*, 788.
(11) Frisch, M. J.; Trucks, G. W.; Schlegel, H. B.; Scuseria, G. E.; Robb, M. A.; Cheeseman, J. R.; Montgomery, J. A., Jr.; Vreven, T.; Kudin, K. N.; Burant, J. C.; Millam, J. M.; Iyengar, S. S.; Tomasi, J.; Barone, V.; Mennucci, B.; Cossi, M.; Scalmani, G.; Rega, N.; Petersson, G. A.; Nakatsuji, H.; Hada, M.; Ehara, M.; Toyota, K.; Fukuda, R.; Hasegawa, J.; Ishida, M.; Nakajima, T.; Honda, Y.; Kitao, O.; Nakai, H.; Klene, M.; Li, X.; Knox, J. E.; Hratchian, H. P.; Cross, J. B.; Adamo, C.; Jaramillo, J.; Gomperts, R.; Stratmann, R. E.; Yazyev, O.; Austin, A. J.; Cammi, R.; Pomelli, C.; Ochterski, J. W.; Ayala, P. Y.; Morokuma, K.; Voth, G. A.; Salvador, P.; Dannenberg, J. J.; Zakrzewski, V. G.; Dapprich, S.; Daniels, A. D.; Strain, M. C.; Farkas, O.; Malick, D. K.; Rabuck, A. D.; Raghavachari, K.; Foresman, J. B.; Ortiz, J. V.; Cui, Q.; Baboul, A. G.; Clifford, S.; Cioslowski, J.; Stefanov, B. B.; Liu, G.; Liashenko, A.; Piskorz, P.; Komaromi, I.; Martin, R. L.; Fox, D. J.; Keith, T.; Al-Laham, M. A.; Peng, C. Y.; Nanayakkara, A.; Challacombe, M.; Gill, P. M. W.; Johnson, B.; Chen, W.; Wong, M. W.; Gonzalez, C.; Pople, J. A. *Gaussian 03*. revision B.04 ed.; Gaussian Inc.: Pittsburgh, PA, 2003.
(12) Pauwels, E.; Van Speybroeck, V.; Waroquier, M. *J. Phys. Chem. A* **2004**, *108*, 11321.
(13) Becke, A. D. J. *J. Chem. Phys.* **1993**, *98*, 5648.
(14) Lee, C.; Yang, W.; Parr, R. G. *Phys. Rev. B* **1988**, 785.
(15) Stevens, P. J.; J., D. F.; Chabalowski, C. F.; Frisch, M. J. *J. Phys. Chem.* **1994**, *98*, 11623.
(16) Reed, A. E.; Weinstock, R. B.; Weinhold, F. J. *J. Phys. Chem.* **1985**, *83*, 735.
(17) Kivan, L.; Kispert, L. D. *Electron Spin Double Resonance Spectroscopy*; John Weily & Sons: New York, 1976.
(18) Sanderud, A.; Sagstuen, E. *J. Phys. Chem. B* **1998**, *102*, 9353.
(19) Heller, C.; McConnell, H. M. *J. Chem. Phys.* **1960**, *32*, 1535.
(20) Morton, J. R. *J. Chem. Rev.* **1964**, *64*, 453.
(21) McConnell, H. M. *J. Chem. Phys.* **1958**, *24*, 764.
(22) Gordy, W. *Theory and Application of Electron Spin Resonance*; John Wiley & Sons: New York, 1980.
(23) Bernhard, W. A. *J. Chem. Phys.* **1984**, *81*, 5928.
(24) Erling, P. A.; Nelson, W. H. *J. Phys. Chem. A* **2004**, *108*, 7591.
(25) Sørnes, A. R.; Sagstuen, E.; Lund, A. *J. Phys. Chem.* **1995**, *99*, 16867.
(26) Sørnes, A.; Sagstuen, E. *J. Phys. Chem.* **1995**, *99*, 16857.
(27) Fouse, G. W.; Bernhard, W. A. *J. Chem. Phys.* **1979**, *70*, 1667.
(28) Hermosilla, L; Calle, P; García de la Vega, P. M; Sieiro, C. *J. Phys. Chem. A* **2005**, *109*, 1114.
(29) Hermosilla, L; Calle, P; García de la Vega, P. M; Sieiro, C. *J. Phys. Chem. A* **2006**, *110*, 13600.